



## Multiple eutectic orientation relationships in undercooled Ni–38wt.%Si eutectic alloy

Fan ZHANG<sup>1</sup>, Hai-feng WANG<sup>1</sup>, Cun LAI<sup>2</sup>, Jian-bao ZHANG<sup>1</sup>, Ya-chan ZHANG<sup>1</sup>, Qing ZHOU<sup>1</sup>

1. Center of Advanced Lubrication and Seal Materials, State Key Laboratory of Solidification Processing, Northwestern Polytechnical University, Xi'an 710072, China;
2. The Third Academy of CASIC, Beijing 100074, China

Received 2 November 2019; accepted 8 June 2020

**Abstract:** Eutectic orientation relationships (EORs) in an undercooled Ni–38wt.%Si alloy were analyzed by electron backscatter diffraction. A total of seven EORs were identified, and three of them were found at the under-cooling degree  $\Delta T \approx 31$  K. It is found that their orientations of the primary NiSi phase are same but the misorientation between the neighboring NiSi<sub>2</sub> grains can be either 50° or 60°. The multiple EORs were ascribed to a possible change in the growth direction of the primary phase, the change of the primary phase from the NiSi phase to the NiSi<sub>2</sub> phase, and the transition from coupled to uncoupled eutectic growth. The current work shows that epitaxial growth of the second eutectic phase on the primary eutectic phase can obey either a single EOR or multiple EORs, which is a unique phenomenon.

**Key words:** eutectic orientation relationship; epitaxial growth; undercooling; Ni–Si alloy

### 1 Introduction

Eutectic alloys have been studied intensively by experiments and modeling due to their practical and theoretical importance [1–9]. Recently, much attention has been paid to the eutectic orientation relationship (EOR) [10–24]. EOR is strongly related to the growth mechanism and thus greatly influences the microstructure and mechanical properties of eutectics. Regarding ceramic oxide eutectics, RAMIREZ-RICO et al [10] studied the texture resulting from the directional solidification of Al<sub>2</sub>O<sub>3</sub>–ZrO<sub>2</sub> (Y<sub>2</sub>O<sub>3</sub>) system and found that the phases grow according to the relationship  $\{10\bar{1}2\}_{\text{Al}_2\text{O}_3} // \{100\}_{\text{ZrO}_2}$ . For directional solidification of NiO–YSZ, CoO–YSZ, NiO–CeO<sub>2</sub>, NiO–GDC, CoO–CeO<sub>2</sub> and CoO–GDC eutectic systems,

ZABALETA et al [11] found two EORs, and the most common of them is  $(111)_{\text{TMO}} // (001)_{\text{IC}}$ ,  $[0\bar{1}1]_{\text{TMO}} // [010]_{\text{IC}}$  (TMO=NiO, CoO; IC=YSZ, GDC, CeO<sub>2</sub>). As one of the most widely used systems for modeling studies of eutectic growth, the Al–Al<sub>2</sub>Cu eutectics formed during directional solidification possess a common EOR of  $(111)_{\text{Al}} // (2\bar{1}1)_{\text{Al}_2\text{Cu}}$ ,  $[\bar{1}10]_{\text{Al}} // [120]_{\text{Al}_2\text{Cu}}$  [12], i.e., the so-called “Beta 6” relationship [13]. Since the Al–Al<sub>3</sub>Ni eutectics could play an important role in thermally stable shape cast alloys and could potentially make aligned fiber composite materials for high-strength applications, their crystallographic orientations and formation mechanisms have been studied [14], and their EOR was found to be  $\{3\bar{1}1\}_{\text{Al}} // \{001\}_{\text{Al}_3\text{Ni}}$ ,  $[110]_{\text{Al}} // [010]_{\text{Al}_3\text{Ni}}$  [15].

Owing to the superior castability, lightmass, high wear resistance and good corrosion resistance,

**Foundation item:** Project (2018-JC007) supported by the Science Fund for Distinguished Young Scholars from Shaanxi Province, China; Project (3102017HQZZ008) supported by the Fundamental Research Funds for the Central Universities, China

**Corresponding author:** Hai-feng WANG; Tel: +86-13519186961; E-mail: haifengw81@nwpu.edu.cn

DOI: 10.1016/S1003-6326(20)65342-0

the Al–Si alloys are the most widely used aluminum casting alloys [19]. One of the important ways to improve their strength and ductility is to change the morphology of the eutectic Si (i.e., from a coarse plate-like microstructure to a fine fibrous microstructure) by adding certain elements (e.g., Sr and Sc) [16–19]. Four types of direction parallelisms between the eutectic  $\alpha(\text{Al})$  and the eutectic Si have been reported, i.e.,  $\langle 001 \rangle_{\text{Al}} // \langle 110 \rangle_{\text{Si}}$ ,  $\langle 001 \rangle_{\text{Al}} // \langle 001 \rangle_{\text{Si}}$ ,  $\langle 112 \rangle_{\text{Al}} // \langle 112 \rangle_{\text{Si}}$  and  $\langle 112 \rangle_{\text{Al}} // \langle 110 \rangle_{\text{Si}}$ . The other way to control the EOR and the eutectic morphology is to modify the processing process. For directional solidification of eutectic alloys, LI et al [21–23] carried out a series of studies to determine the effects of a high magnetic field on the morphologies and orientations of the primary phase and the eutectic phases. Taking the Al–Al<sub>3</sub>Ni eutectic alloy as an example, the EOR changes from  $\{311\}_{\text{Al}} // \{001\}_{\text{Al}_3\text{Ni}}$ ,  $[110]_{\text{Al}} // [010]_{\text{Al}_3\text{Ni}}$  without a magnetic field to  $\{001\}_{\text{Al}} // \{102\}_{\text{Al}_3\text{Ni}}$ , and  $[102]_{\text{Al}} // [010]_{\text{Al}_3\text{Ni}}$  with a high magnetic field [21].

The investigation was also done to characterize the EORs of ternary eutectics [24]. For directional solidification of an Al–Ag–Cu alloy, two different sets of EORs were identified among the  $\alpha(\text{Al})$ , Al<sub>2</sub>Cu and Ag<sub>2</sub>Al phases, i.e.,  $\{130\}_{\text{Al}} // \{100\}_{\text{Al}_2\text{Cu}}$ ,  $\{110\}_{\text{Al}_2\text{Cu}} // \{10\bar{1}0\}_{\text{Ag}_2\text{Al}}$  and  $\{130\}_{\text{Al}} // \{100\}_{\text{Al}_2\text{Cu}}$ ,  $\{140\}_{\text{Al}_2\text{Cu}} // \{0001\}_{\text{Ag}_2\text{Al}}$ . The less common EOR of  $\{130\}_{\text{Al}} // \{100\}_{\text{Al}_2\text{Cu}}$  was found in the ternary Al–Ag–Cu alloy, indicating that the presence of the Ag<sub>2</sub>Al phase stabilizes this particular EOR.

All of the previously mentioned researches on EORs [10–24] focused on directional solidification and casting, and in this case, the growth velocity is small, and the interface is under local equilibrium conditions. However, with an increase in velocity, the interface becomes under non-equilibrium conditions, leading to the significant changes in the interface dynamics and the eutectic morphologies [1]. It should be noted that the non-equilibrium solidification is a useful method to control and enrich eutectic microstructures. For example, an important non-equilibrium phenomenon in undercooled eutectic alloy melts is the transition from regular lamellar to anomalous eutectics [5–9]. Taking into account the important role of orientation relationships on eutectic growth [10–25], the present work aimed at reporting the EORs in undercooled alloys.

In this work, the EORs in undercooled Ni–38wt.%Si alloy, with two stoichiometric intermetallic compounds (i.e., NiSi and NiSi<sub>2</sub> [15]) as eutectic products, were identified by using the electron backscatter diffraction (EBSD). For the Ni–38wt.%Si eutectic alloy with different undercooling degrees and microstructures, the interplay relationships between the EORs and the eutectic morphologies were discussed. Special attention was paid to the growth mechanism of the eutectics. The present work shows that epitaxial growth of a second eutectic phase on the first eutectic phase can obey either a single EOR or multiple EORs and helps understand eutectic growth and eutectic morphologies.

## 2 Experimental

A high-purity ingot with a mass of approximately 50 g and a nominal eutectic composition of Ni–38wt.%Si was prepared from pure nickel (99.99%) and silicon (99.999%). The melt flux technique was used to undercool the Ni–38wt.%Si eutectic alloy. A quartz-glass crucible, which was rinsed previously in an alcoholic solution by an ultrasonic cleaning machine, was used as the container. The master alloy was re-melted at least three times in an arc furnace under a high-purity Ar atmosphere to ensure chemical homogeneity. A sample with mass of approximately 2 g was cut from the master alloy, and then placed into the quartz-glass crucible with a certain quantity of boron oxide glass flux. The quartz-glass crucible was positioned within the high-frequency induction coil of a chamber that was first evacuated to a pressure of  $3 \times 10^{-3}$  Pa and then backfilled with high-purity Ar gas to a pressure of  $5 \times 10^{-2}$  MPa. The sample, covered by the melt flux, was heated to 100–250 K above the eutectic temperature and held at that temperature for approximately 20 min. Each sample was cyclically superheated and cooled until the desired undercooling degree was achieved.

The as-solidified sample was mounted in Bakelite and carefully polished. After etching in a solution of 10 mL H<sub>2</sub>O<sub>2</sub>, 10 mL HCl, and 50 mL H<sub>2</sub>O, the sample was observed with an optical microscope (Olympus GX71) to examine various eutectic microstructures. After polishing the sample with a SiO<sub>2</sub> colloidal suspension in a vibratory

polisher, the crystallographic orientations were studied using a scanning electron microscope (TESCAN MIRA 3 XMU) equipped with an EBSD analysis system. Using the software Channel 5 Suite and Material Studio 8.0, the models for the spatial distribution of the lattices were established to examine the EORs directly.

Since the compositions of eutectic products, NiSi and NiSi<sub>2</sub> phases, do not change with undercooling degree, the chemical superheating effect [26] is eliminated, and the reduction of interfacial energy is left as the only driving force for re-melting. Furthermore, there is no phase transformation except for eutectic solidification in this alloy system. Consequently, the initial eutectic solidification microstructures can be completely or at least partially retained to room temperature to identify the EORs that occur during non-equilibrium solidification.

### 3 Results

The maximal undercooling degree achieved in the present work is  $\Delta T \approx 74$  K. To examine the microstructure evolution, the as-solidified sample with an undercooling degree interval of approximately 5 K was retained to room temperature. Five different microstructures were found among undercooling degrees of approximately 3, 15, 31, 51 and 74 K. The EOR is generally demonstrated by the parallel crystal plane and the parallel crystal direction in the parallel crystal plane [10–24]. According to the geometry of pole figures (PFs), if the poles overlap in the PFs of two eutectic phases, their corresponding lattice planes or crystal orientations are parallel. EBSD was used to characterize the crystallographic orientations of the NiSi and NiSi<sub>2</sub> phases to determine the EORs for the five different microstructures, as seen in Figs. 1–7, in which the parallel crystal planes and directions between the NiSi and NiSi<sub>2</sub> phases are depicted using the software Channel 5 Suite and Material Studio 8.0, and the large and small spheres represent the Ni and Si atoms, respectively.

#### 3.1 Single EOR at $\Delta T \approx 3$ K

For  $\Delta T \approx 3$  K, the microstructure of the Ni–38wt.%Si eutectic alloy is a typical thin and regular lamellar eutectic (Figs. 1(a<sub>1</sub>) and (a<sub>2</sub>)). From

the EBSD orientation maps, only one main orientation was found for the NiSi (Fig. 1(a<sub>1</sub>)) and the NiSi<sub>2</sub> (Fig. 1(a<sub>2</sub>)) phases, which is consistent with the cooperative growth of lamellar eutectics. For the PFs of the NiSi and NiSi<sub>2</sub> phases in Figs. 1(b<sub>1</sub>) and (b<sub>2</sub>), there is an overlap between  $\{110\}_{\text{NiSi}}$  and  $\{112\}_{\text{NiSi}_2}$ ,  $\langle 1\bar{1}1 \rangle_{\text{NiSi}}$  and  $\langle 1\bar{1}0 \rangle_{\text{NiSi}_2}$ , indicating that the corresponding EOR is  $\{110\}_{\text{NiSi}} // \{112\}_{\text{NiSi}_2}$ ,  $\langle 1\bar{1}1 \rangle_{\text{NiSi}} // \langle 1\bar{1}0 \rangle_{\text{NiSi}_2}$ . The fore-named EOR is demonstrated by the families of the crystal planes and directions. A model for the spatial distribution of the lattices needs to be established to obtain the parallel crystal plane and the parallel crystal direction in the parallel crystal plane. Figures 1(c<sub>1</sub>) and (c<sub>2</sub>) show schematic diagrams of the EOR at  $\Delta T \approx 3$  K. The pink crystal plane and crystal direction are the parallel crystal plane and parallel crystal direction in the parallel crystal plane, i.e.,  $(110)_{\text{NiSi}} // (112)_{\text{NiSi}_2}$ ,  $[1\bar{1}1]_{\text{NiSi}} // [1\bar{1}0]_{\text{NiSi}_2}$ . In this case, only one single EOR can be identified.

#### 3.2 Single EOR at $\Delta T \approx 15$ K

For  $\Delta T \approx 15$  K, a directional and granular primary NiSi phase is surrounded by a thin and regular lamellar eutectic (Figs. 2(a<sub>1</sub>) and (a<sub>2</sub>)). From the EBSD orientation maps and PFs, three orientations can be found for the primary NiSi phase. Since the granular structures and the surrounding regular lamellae of the NiSi phase share the same orientation, the lamellar eutectics are formed by an epitaxial growth mechanism. Correspondingly, the regular lamellae of the NiSi<sub>2</sub> phase also have three orientations. The differences among the three orientations are not large ( $\leq 5^\circ$ ), and thus it is reasonable to integrate them into one orientation. Using this approach, only one orientation can be found for the NiSi (Fig. 2(a<sub>1</sub>)) and NiSi<sub>2</sub> (Fig. 2(a<sub>2</sub>)) phases, and there is an overlap between  $\{\bar{1}1\bar{1}\}_{\text{NiSi}}$  and  $\{101\}_{\text{NiSi}_2}$ , and  $\langle \bar{1}10 \rangle_{\text{NiSi}}$  and  $\langle 11\bar{1} \rangle_{\text{NiSi}_2}$  (Figs. 2(b<sub>1</sub>) and (b<sub>2</sub>)), indicating that the corresponding EOR is  $\{\bar{1}1\bar{1}\}_{\text{NiSi}} // \{101\}_{\text{NiSi}_2}$ ,  $\langle \bar{1}10 \rangle_{\text{NiSi}} // \langle 11\bar{1} \rangle_{\text{NiSi}_2}$ . Figures 2(c<sub>1</sub>) and (c<sub>2</sub>) show the schematic diagrams of the EOR at  $\Delta T \approx 15$  K. The blue crystal plane and crystal direction are the parallel crystal plane and parallel crystal direction in the parallel crystal plane, i.e.,  $(\bar{1}1\bar{1})_{\text{NiSi}} // (101)_{\text{NiSi}_2}$ ,  $[\bar{1}10]_{\text{NiSi}} // [11\bar{1}]_{\text{NiSi}_2}$ . Only one EOR can be identified.

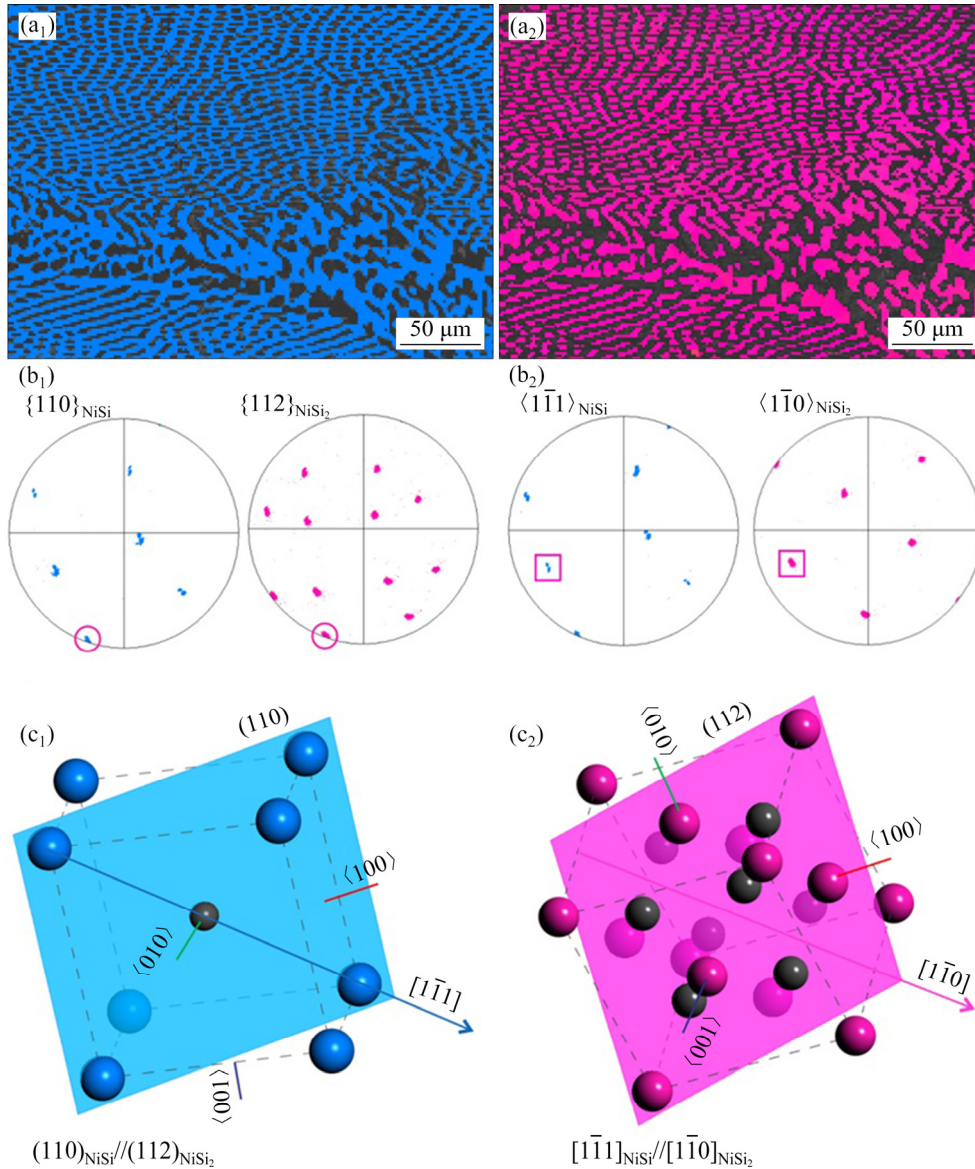


**Fig. 1** EBSD orientation maps and eutectic orientation relationships of Ni–38wt.%Si alloy at  $\Delta T \approx 3$  K: (a<sub>1</sub>, a<sub>2</sub>) EBSD orientation maps of NiSi (a<sub>1</sub>) and NiSi<sub>2</sub> (a<sub>2</sub>) phases; (b<sub>1</sub>, b<sub>2</sub>) Overlap between  $\{110\}_{\text{NiSi}}$  and  $\{112\}_{\text{NiSi}_2}$  (b<sub>1</sub>), and  $\langle 1\bar{1}1 \rangle_{\text{NiSi}}$  and  $\langle 1\bar{1}0 \rangle_{\text{NiSi}_2}$  (b<sub>2</sub>); (c<sub>1</sub>, c<sub>2</sub>) Parallel crystal planes and directions between NiSi (c<sub>1</sub>) and NiSi<sub>2</sub> (c<sub>2</sub>) phases

### 3.3 Triple EORs at $\Delta T \approx 31$ K

For  $\Delta T \approx 31$  K, the primary NiSi phase is surrounded by a coarse eutectic structure, and the rest of the microstructure is composed of a thin and regular lamellar eutectic, as seen in the EBSD orientation maps in Figs. 3(a) and (c). The  $\{100\}$  PFs are shown in Figs. 3(b) and (d). For the NiSi phase, only one orientation can be identified (Fig. 3(b)), indicating that both the coarse eutectic structures and the thin and regular lamellar eutectics are formed by epitaxial growth after the solidification of the primary NiSi phase (Fig. 3(a)). For the NiSi<sub>2</sub> phase, however, three main orientations can be found, and the orientation

differences between them are rather large (Figs. 3(c) and (d)). The blue, green and pink grains are labeled as “A”, “B” and “C”, respectively, in Fig. 3(c). The blue and green (and the green and pink) grains share one concentrated pole in the  $\{100\}$  PF (Fig. 3(d)). Three other grains are labeled “A’”, “B’” and “C’”. The orientation differences among grains A, B, and C and grains A’, B’, and C’, respectively, are so small ( $\leq 5^\circ$ ) that they are not considered in the following analysis of EORs. These EBSD results suggest that there are three different EORs when  $\Delta T \approx 31$  K. Since the NiSi<sub>2</sub> grains are rather large ( $>200 \mu\text{m}$ ), such three EORs should be formed by the eutectic solidification itself

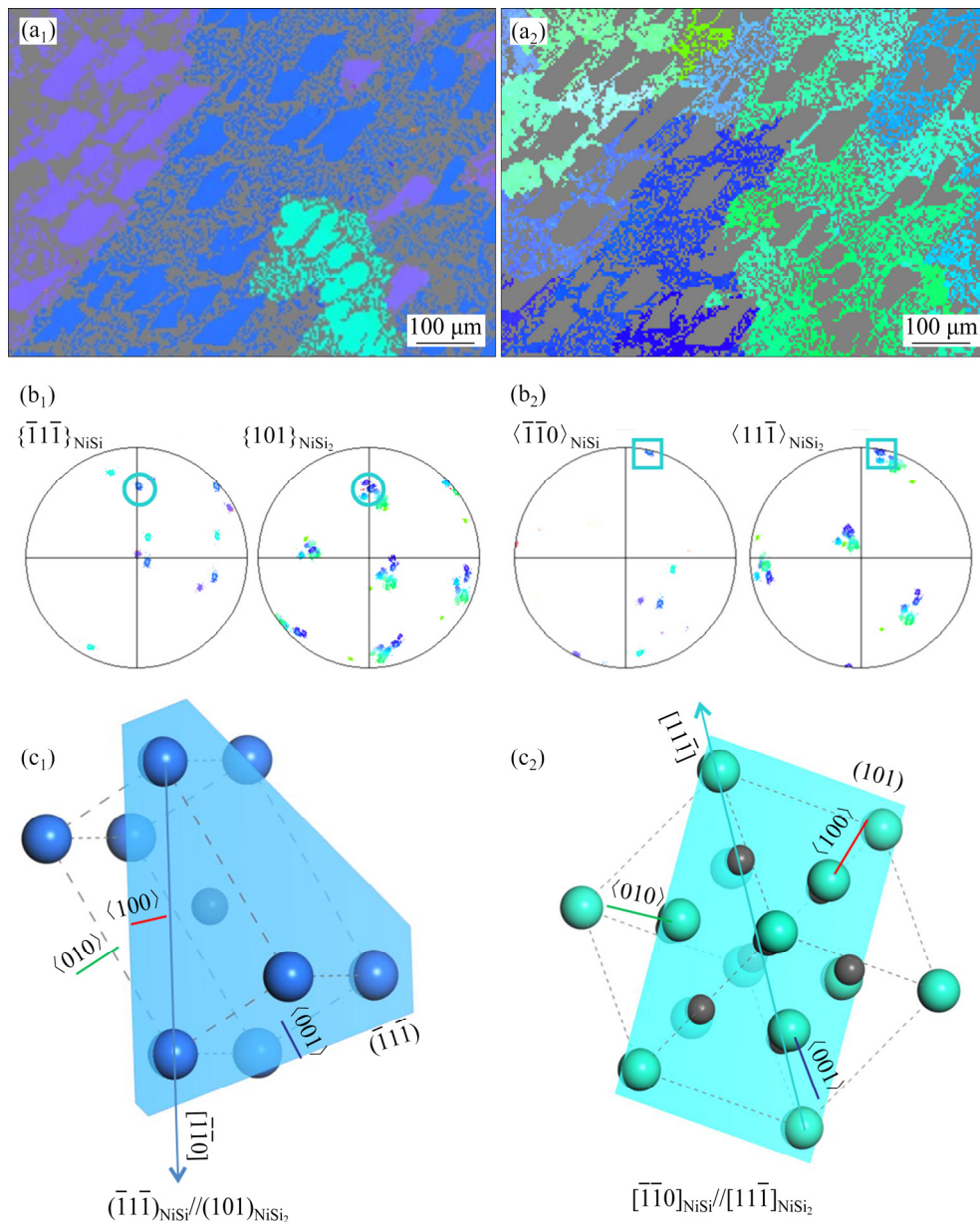


**Fig. 2** EBSD orientation maps and eutectic orientation relationships of Ni–38wt.%Si alloy at  $\Delta T \approx 15$  K: (a<sub>1</sub>, a<sub>2</sub>) EBSD orientation maps of NiSi (a<sub>1</sub>) and NiSi<sub>2</sub> (a<sub>2</sub>) phases; (b<sub>1</sub>, b<sub>2</sub>) Overlap between  $\{111\}_{\text{NiSi}}$  and  $\{101\}_{\text{NiSi}_2}$  (b<sub>1</sub>), and  $\langle 110 \rangle_{\text{NiSi}}$  and  $\langle 111 \rangle_{\text{NiSi}_2}$  (b<sub>2</sub>); (c<sub>1</sub>, c<sub>2</sub>) Parallel crystal planes and directions between NiSi (c<sub>1</sub>) and NiSi<sub>2</sub> (c<sub>2</sub>) phases

and should not be a result of re-melting, convection or solidification stresses that could considerably change the grain orientations [27–32].

To determine the EORs, PFs of the NiSi and NiSi<sub>2</sub> phases when  $\Delta T \approx 31$  K are shown in Fig. 4. For the NiSi phase from Fig. 3(a) and grain A from Fig. 3(c), there is an overlap between  $\{100\}_{\text{NiSi}}$  and  $\{010\}_{\text{NiSi}_2}$  (Fig. 4(a<sub>1</sub>)),  $\langle 010 \rangle_{\text{NiSi}}$  and  $\langle 10\bar{1} \rangle_{\text{NiSi}_2}$  (Fig. 4(a<sub>2</sub>)), indicating that the corresponding EOR is  $\{100\}_{\text{NiSi}} // \{010\}_{\text{NiSi}_2}$ ,  $\langle 010 \rangle_{\text{NiSi}} // \langle 10\bar{1} \rangle_{\text{NiSi}_2}$ . Similarly, the EORs between

the NiSi phase from Fig. 3(a) and grains B and C from Fig. 3(c) are  $\{10\bar{1}\}_{\text{NiSi}} // \{110\}_{\text{NiSi}_2}$ ,  $\langle 11\bar{1} \rangle_{\text{NiSi}} // \langle 11\bar{1} \rangle_{\text{NiSi}_2}$  and  $\{111\}_{\text{NiSi}} // \{1\bar{1}\}_{\text{NiSi}_2}$ ,  $\langle 01\bar{1} \rangle_{\text{NiSi}} // \langle 10\bar{1} \rangle_{\text{NiSi}_2}$ , as seen in Figs. 4(b<sub>1</sub>), (b<sub>2</sub>) and Figs. 4(c<sub>1</sub>), (c<sub>2</sub>), respectively. Figure 5 shows the schematic diagrams of the three EORs when  $\Delta T \approx 31$  K. For the NiSi phase from Fig. 3(a) and grain A from Fig. 3(c), the blue crystal plane and crystal direction are the parallel crystal plane and parallel crystal direction in the parallel crystal plane (Figs. 5(a) and (b<sub>1</sub>)), i.e.,  $(100)_{\text{NiSi}} // (010)_{\text{NiSi}_2}$ ,

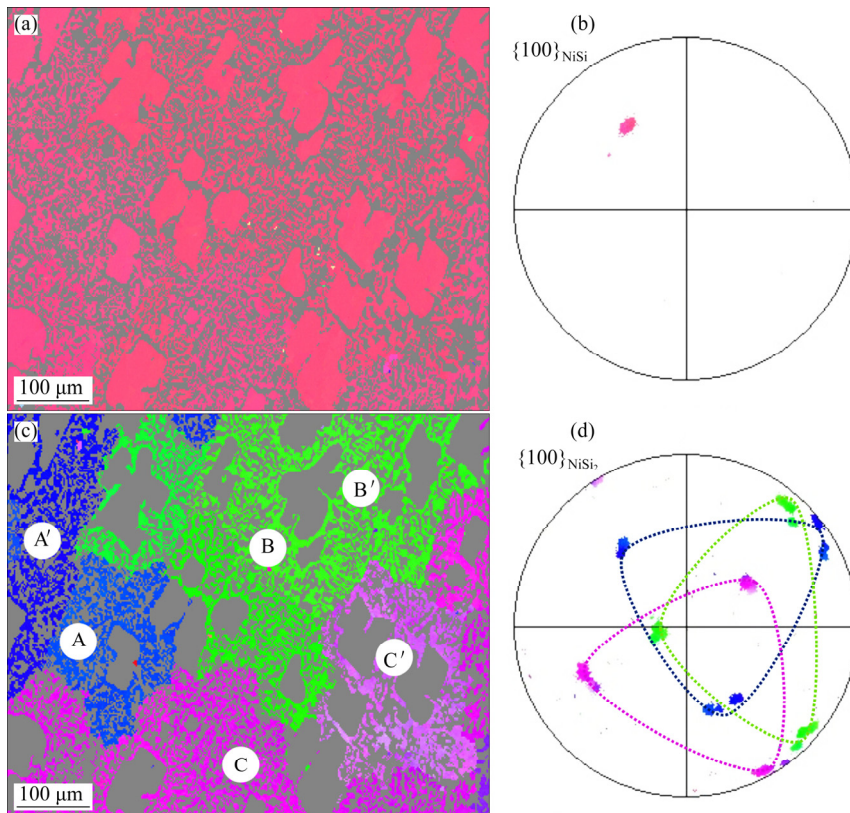


**Fig. 3** EBSD analysis of eutectic microstructure in undercooled Ni–38wt.%Si alloy at  $\Delta T \approx 31$  K: (a, c) EBSD orientation maps; (b, d)  $\{100\}$  PFs of NiSi (a, b) and NiSi<sub>2</sub> (c, d) phases

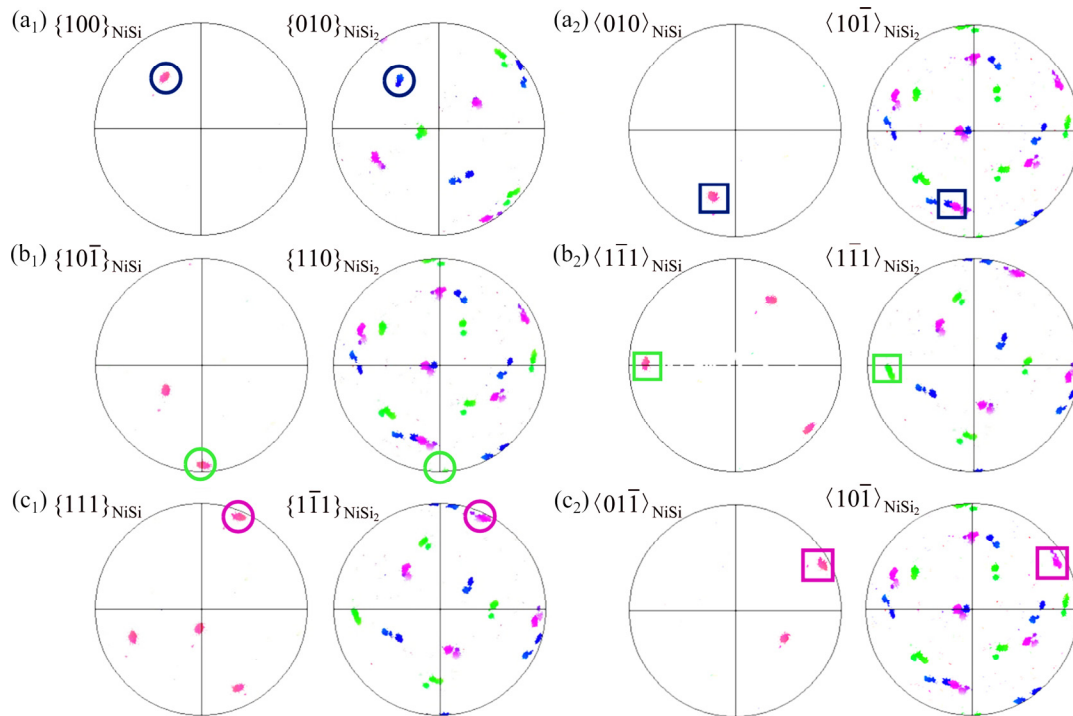


**Fig. 4** Three eutectic orientation relationships in undercooled Ni–38wt.%Si alloy at  $\Delta T \approx 31$  K: (a<sub>1</sub>, a<sub>2</sub>) Overlap between poles in PFs of NiSi phase from Fig. 3(a) and grain A from Fig. 3(c); (b<sub>1</sub>, b<sub>2</sub>) Overlap between poles in PFs of NiSi phase from Fig. 3(a) and grain B from Fig. 3(c); (c<sub>1</sub>, c<sub>2</sub>) Overlap between poles in PFs of NiSi phase from Fig. 3(a) and grain C from Fig. 3(c)

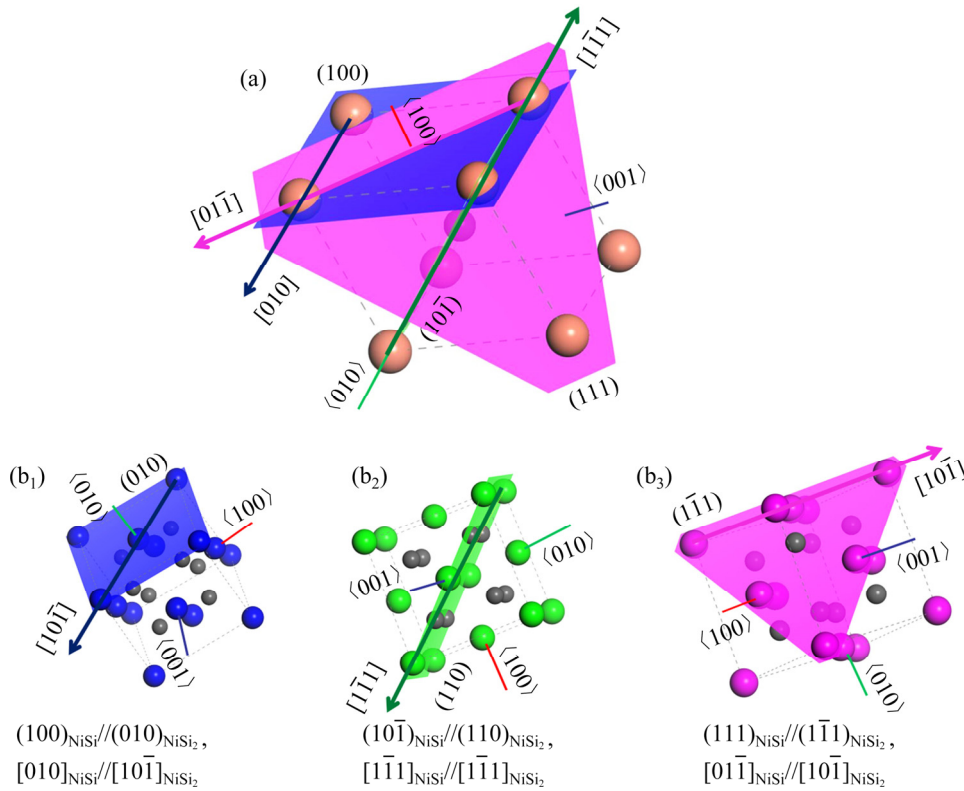


**Fig. 5** Schematic diagrams of three EORs in undercooled Ni–38wt.%Si alloy at  $\Delta T \approx 31$  K: (a) NiSi phase; (b<sub>1</sub>–b<sub>3</sub>) NiSi<sub>2</sub> phase

$[010]_{NiSi} // [10\bar{1}]_{NiSi_2}$ . Similarly, the green crystal plane and crystal direction correspond to the NiSi phase from Fig. 3(a) and grain B from Fig. 3(c), and the EOR is  $(10\bar{1})_{NiSi} // (110)_{NiSi_2}$ ,  $[1\bar{1}1]_{NiSi} // [1\bar{1}1]_{NiSi_2}$ ; the pink crystal plane and crystal direction correspond to the NiSi phase from Fig. 3(a) and grain C from Fig. 3(c), and the EOR is  $(111)_{NiSi} // (1\bar{1}1)_{NiSi_2}$ ,  $[01\bar{1}]_{NiSi} // [10\bar{1}]_{NiSi_2}$ , as seen in Figs. 5(a), (b<sub>2</sub>) and (b<sub>3</sub>), respectively. Three EORs co-exist in the same sample when  $\Delta T \approx 31$  K. The green crystal planes in Figs. 5(a) and (b<sub>2</sub>) are not easily distinguished due to the viewing angle. The orientation differences between the three NiSi<sub>2</sub> grains A, B and C can be obtained from the misorientation between the neighboring grains. For grains A and B (B and C), which share one concentrated pole in the  $\{100\}$  PF (Fig. 3(d)), the misorientation is approximately 50°. For grains A and C, which do not share a concentrated pole in the  $\{100\}$  PF (Fig. 3(d)), the misorientation is approximately 60°.

**3.4 Single EOR at  $\Delta T \approx 51$  K**

For  $\Delta T \approx 51$  K, strip-shaped NiSi structures and dendritic NiSi<sub>2</sub> grains are found as well as the thin

and regular lamellar eutectics (Figs. 6(a<sub>1</sub>) and (a<sub>2</sub>)). From the EBSD orientation maps and PFs, only one orientation can be found for the NiSi (Fig. 6(a<sub>1</sub>)) and NiSi<sub>2</sub> (Fig. 6(a<sub>2</sub>)) phases, and there is an overlap between  $\{\bar{1}10\}_{NiSi}$  and  $\{100\}_{NiSi_2}$  (Fig. 6(b<sub>1</sub>)),  $\langle 111 \rangle_{NiSi}$  and  $\langle \bar{1}10 \rangle_{NiSi_2}$  (Fig. 6(b<sub>2</sub>)), indicating that the corresponding EOR is  $\{\bar{1}10\}_{NiSi} // \{100\}_{NiSi_2}$ ,  $\langle 111 \rangle_{NiSi} // \langle \bar{1}10 \rangle_{NiSi_2}$ . The schematic diagrams of EOR when  $\Delta T \approx 51$  K are shown in Figs. 6(c<sub>1</sub>) and (c<sub>2</sub>). The green crystal plane and crystal direction are the parallel crystal plane and parallel crystal direction in the parallel crystal plane, i.e.,  $(\bar{1}10)_{NiSi} // (100)_{NiSi_2}$ ,  $[111]_{NiSi} // [\bar{1}10]_{NiSi_2}$ . When  $\Delta T \approx 51$  K, only one EOR can be found.

**3.5 Single EOR at  $\Delta T \approx 74$  K**

When  $\Delta T \approx 74$  K, re-melting induces anomalous eutectics that make the orientations random, aside from which only one orientation was found for the NiSi and the NiSi<sub>2</sub> phases, as seen in Figs. 7(a<sub>1</sub>) and (a<sub>2</sub>). As previously mentioned, the eutectic products of undercooled Ni–38wt.%Si alloy are two stoichiometric intermetallic compounds (i.e., NiSi and NiSi<sub>2</sub>) [25], whose compositions do not change

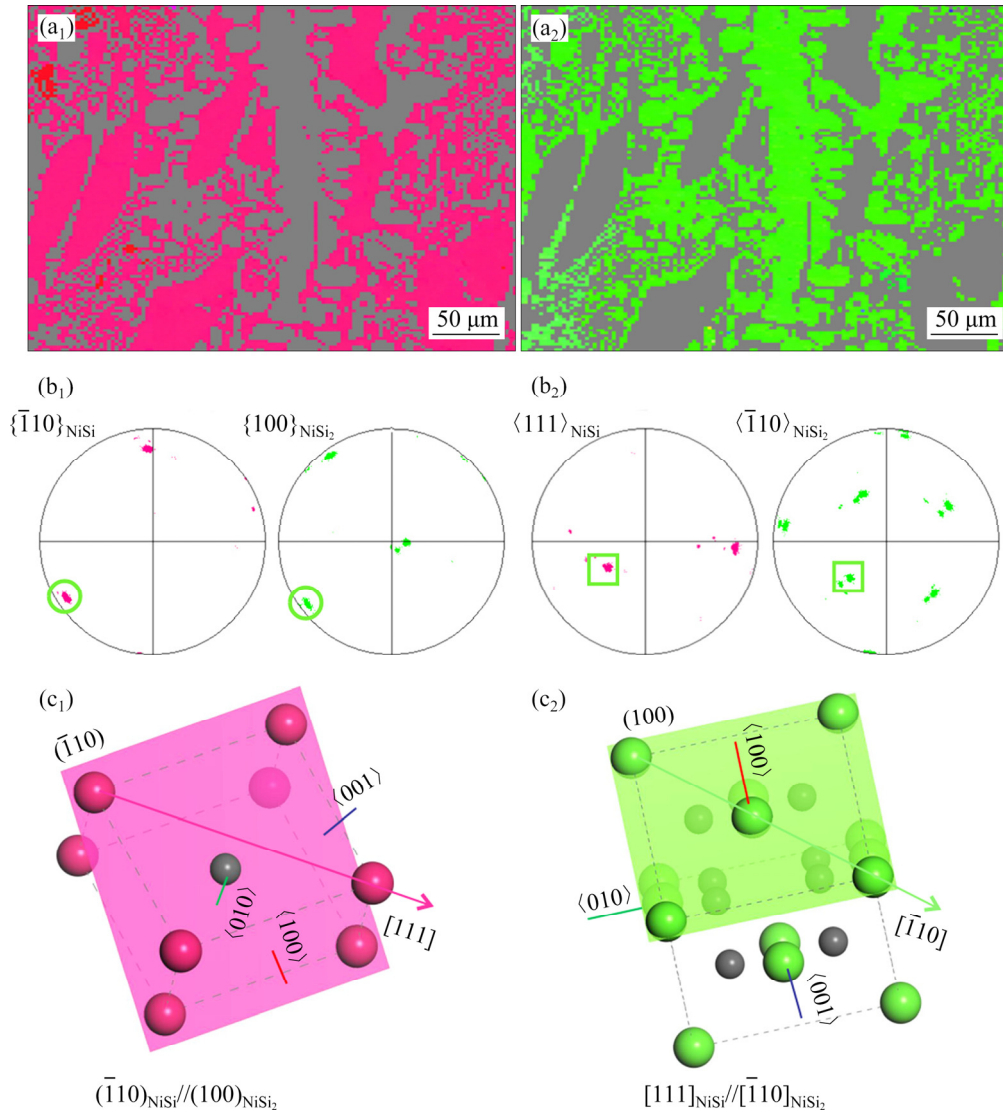


**Fig. 6** EBSD orientation maps and eutectic orientation relationships of Ni–38wt.%Si alloy at  $\Delta T \approx 51$  K: (a<sub>1</sub>, a<sub>2</sub>) EBSD orientation maps of NiSi (a<sub>1</sub>) and NiSi<sub>2</sub> (a<sub>2</sub>) phases; (b<sub>1</sub>, b<sub>2</sub>) Overlap between  $\{110\}_{\text{NiSi}}$  and  $\{100\}_{\text{NiSi}_2}$  (b<sub>1</sub>),  $\langle 111 \rangle_{\text{NiSi}}$  and  $\langle 110 \rangle_{\text{NiSi}_2}$  (b<sub>2</sub>); (c<sub>1</sub>, c<sub>2</sub>) Parallel crystal planes and directions between NiSi (c<sub>1</sub>) and NiSi<sub>2</sub> (c<sub>2</sub>) phases

with undercooling degree. Consequently, the initial eutectic microstructure can be completely or at least partially retained to room temperature to exhibit the original EOR that governs non-equilibrium solidification. As shown in Figs. 7(b<sub>1</sub>) and (b<sub>2</sub>), the corresponding EOR is  $\{111\}_{\text{NiSi}} // \{011\}_{\text{NiSi}_2}$ ,  $\langle 110 \rangle_{\text{NiSi}} // \langle 011 \rangle_{\text{NiSi}_2}$ . Figures 7(c<sub>1</sub>) and (c<sub>2</sub>) show the schematic diagrams of the EOR of Ni–38wt.%Si alloy when  $\Delta T \approx 74$  K. The red crystal plane and crystal direction are the parallel crystal plane and parallel crystal direction in the parallel crystal plane (Figs. 7(c<sub>1</sub>) and (c<sub>2</sub>)), i.e.,  $(111)_{\text{NiSi}} // (011)_{\text{NiSi}_2}$ ,  $[\bar{1}10]_{\text{NiSi}} // [011]_{\text{NiSi}_2}$ . Only one EOR can be identified.

All of the microstructures and the EORs

characterized in the present work are summarized in Table 1. There are no identical EORs for different undercooling degrees with different microstructures. When  $\Delta T \approx 15$  and 31 K, the second NiSi<sub>2</sub> phase grows epitaxially on the primary NiSi phase (Figs. 2 and 3). Since the regular lamellar eutectics are formed during the post-recalence stage when  $\Delta T \approx 3, 15$  and 31 K [9], their growth mechanisms and EORs should be the same, but this is not the case. When  $\Delta T \approx 51$  K, strip-shaped NiSi structures and dendritic NiSi<sub>2</sub> grains co-exist (Fig. 6). In this case, the epitaxial growth of the NiSi phase on the NiSi<sub>2</sub> phase and epitaxial growth of the NiSi<sub>2</sub> phase on the NiSi phase occur concurrently. Two different EORs are expected, but in fact, only one EOR can

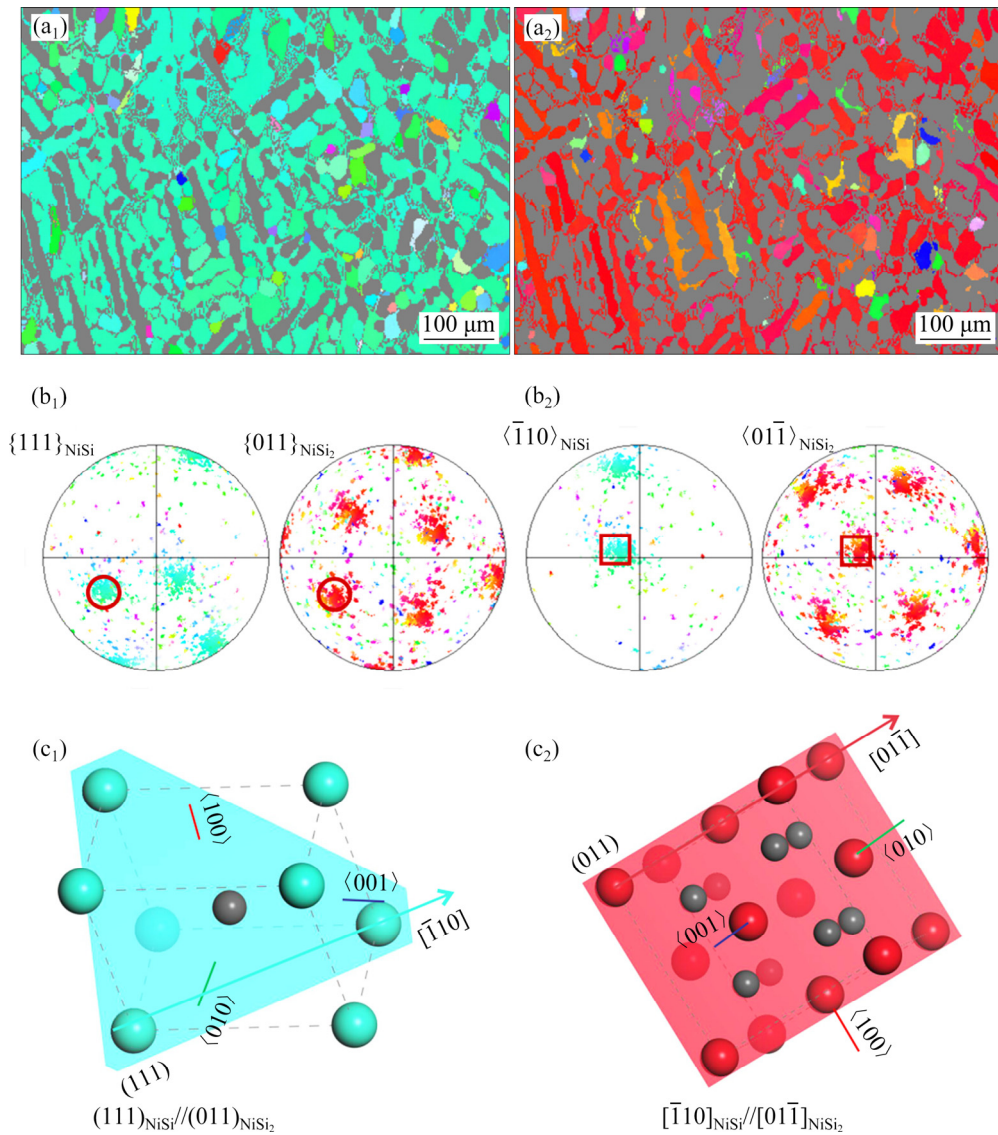


**Fig. 7** EBSD orientation maps and eutectic orientation relationships of Ni–38wt.%Si alloy at  $\Delta T \approx 74$  K: (a<sub>1</sub>, a<sub>2</sub>) EBSD orientation maps of NiSi (a<sub>1</sub>) and NiSi<sub>2</sub> (a<sub>2</sub>) phases; (b<sub>1</sub>, b<sub>2</sub>) Overlap between  $\{111\}_{NiSi}$  and  $\{011\}_{NiSi_2}$  (b<sub>1</sub>),  $\langle \bar{1}10 \rangle_{NiSi}$  and  $\langle 01\bar{1} \rangle_{NiSi_2}$  (b<sub>2</sub>); (c<sub>1</sub>, c<sub>2</sub>) Parallel crystal planes and directions between NiSi (c<sub>1</sub>) and NiSi<sub>2</sub> (c<sub>2</sub>) phases

**Table 1** Microstructures and EORs in undercooled Ni–38wt.%Si alloy

Undercooling degree/K	Microstructure	Eutectic orientation relationship
~3	Regular lamellar eutectics	$(110)_{NiSi} // (112)_{NiSi_2}$ , $[1\bar{1}\bar{1}]_{NiSi} // [1\bar{1}0]_{NiSi_2}$
~15	Primary NiSi phase surrounded by regular lamellar eutectics	$(\bar{1}\bar{1}\bar{1})_{NiSi} // (101)_{NiSi_2}$ , $[\bar{1}\bar{1}0]_{NiSi} // [11\bar{1}]_{NiSi_2}$
~31	Primary NiSi phase surrounded successively by coarse and thin lamellar eutectics	$(100)_{NiSi} // (010)_{NiSi_2}$ , $[010]_{NiSi} // [10\bar{1}]_{NiSi_2}$ ; $(10\bar{1})_{NiSi} // (110)_{NiSi_2}$ , $[1\bar{1}\bar{1}]_{NiSi} // [1\bar{1}\bar{1}]_{NiSi_2}$ ; $(111)_{NiSi} // (1\bar{1}1)_{NiSi_2}$ , $[01\bar{1}]_{NiSi} // [10\bar{1}]_{NiSi_2}$
~51	Strip-shaped NiSi and dendritic NiSi <sub>2</sub> surrounded by regular lamellar eutectics	$(\bar{1}10)_{NiSi} // (100)_{NiSi_2}$ , $[111]_{NiSi} // [\bar{1}10]_{NiSi_2}$
~74	Eutectic dendrites and anomalous eutectics	$(111)_{NiSi} // (011)_{NiSi_2}$ , $[\bar{1}10]_{NiSi} // [01\bar{1}]_{NiSi_2}$

be found. When  $\Delta T \approx 74$  K, the epitaxial growth of the NiSi phase on the NiSi<sub>2</sub> dendrites forms a eutectic-dendrite, and an additional EOR is found. The current multiple EORs in the undercooled Ni–38wt.%Si eutectic alloy seem quite anomalous. It should be noted that when  $\Delta T \approx 15$  and 74 K, points in the PFs of NiSi and NiSi<sub>2</sub> phases are rather large which might determine current EORs plausible (see Figs. 2 and 7). Actually, with the help of the software Channel 5, we can find that the PFs of neighboring NiSi and NiSi<sub>2</sub> grains and the EORs are the same as what shown in Figs. 2 and 7.

## 4 Discussion

### 4.1 EORs vs eutectic morphologies

For dendritic growth that involves only one kind of bulk phase and interface, the morphology is strongly related to the interface dynamics, and it is well known that the anisotropy of interface energy plays an important role in pattern formation [1]. Since the interface energy is different for different interface planes, the anisotropy of interface energy can be reflected in the growth direction. For example, several dendrite orientations have been identified in undercooled Cu–8.9wt.%Ni alloys, i.e., fully  $\langle 100 \rangle$ -oriented at low undercooling degree, mixed  $\langle 100 \rangle / \langle 111 \rangle$ -oriented at intermediate undercooling degree and fully  $\langle 111 \rangle$ -oriented at high undercooling degree [33,34]. The existence of competing anisotropies in different growth directions at intermediate undercooling degree gives rise to seaweed dendrite, which is characterized by its containment within a diverging split primary dendrite branch. In addition to the anisotropy of the interface energy, kinetic anisotropy also plays an important role in pattern formation [35] and can dominate if deviations from the local equilibrium conditions are significant. Therefore, the dendrite morphology might be influenced by two factors during non-equilibrium solidification, which are the anisotropy of the interface energy and the kinetic anisotropy.

Eutectic growth involves not only bulk phases and interfaces but also triple-junctions [3]. Taking the solidification of binary eutectics  $L \rightarrow \alpha + \beta$  as an example, there are three kinds of bulk phases (two solids,  $\alpha$  and  $\beta$ , and one liquid,  $L$ ), three kinds of interfaces ( $\alpha/L$ ,  $\beta/L$  and  $\alpha/\beta$ ) and one kind of triple-junction ( $\alpha/\beta/L$ ). Similar to dendrites, the

interface dynamics plays an important role in pattern formation [36], and the anisotropy of the interface energies and the kinetic anisotropy should be considered simultaneously for non-equilibrium solidification of eutectic alloys. The dendrites have only one kind of solid/liquid interface, while there are two kinds of solid/liquid interfaces in the solidification of a binary eutectic, the  $\alpha/L$  and  $\beta/L$  interfaces, for which the anisotropies of the interface energies can determine the growth directions. Furthermore, there is also one solid/solid interface, i.e., the  $\alpha/\beta$  interface, whose interface energy anisotropy can be reflected by the EOR.

There is one kind of triple-junction,  $\alpha/\beta/L$ . Recent work has shown that the triple-junction possesses specific line energy [37], which is different for different crystallography of tri-crystals [38], similar to the interface energy. For eutectic solidification, various eutectic patterns are considerably influenced by the kinetics of triple-junctions. One example is the experimental study of the CBr<sub>4</sub>–C<sub>2</sub>Cl<sub>6</sub> eutectic system [39,40]. In contrast to the classical stability theory [41,42], a lamellar pattern can be stable with a lamellar spacing that is smaller than that predicted by the minimum undercooling principle. Although the deviation of the contact angles from the eutectic interface normal direction is too small (e.g., 1°) to be detected, its significant effect on the stability is precisely measurable [40]. If triple-junctions are allowed to grow in not only normal but also lateral directions, the overstability of lamellar eutectic growth can be successfully explained [39,40].

The eutectic morphology might be controlled by eight separate factors during non-equilibrium solidification, which include the anisotropies of the interface energies and the kinetic anisotropies of the  $\alpha/L$ ,  $\beta/L$  and  $\alpha/\beta$  interfaces and the anisotropy of the line energy and the kinetic anisotropy of the  $\alpha/\beta/L$  triple-junction. Since the EOR is only one of the eight factors that may influence the eutectic morphology, it helps understand the eutectic microstructures but cannot be assumed to be the only factor that dominates the eutectic morphologies.

In the present work, the EORs are different for different eutectic microstructures. When  $\Delta T \approx 15$  and 31 K, the eutectic NiSi phase grows epitaxially from the primary NiSi phase, and then the eutectic NiSi<sub>2</sub> phase grows epitaxially from the eutectic

NiSi phase, as seen in Figs. 2 and 3. When  $\Delta T \approx 74$  K, the NiSi phase grows epitaxially from the primary NiSi<sub>2</sub> phase, as seen in Fig. 7. Both the lamellar eutectics seen when  $\Delta T \approx 15$  and 31 K and the eutectic dendrites seen when  $\Delta T \approx 74$  K follow an epitaxial growth mechanism that obeys a specific EOR or EORs. The random orientation seen when  $\Delta T \approx 74$  K should be a result of re-melting, convection or solidification stresses [27–32] and cannot be taken as the characteristic of eutectic growth. When  $\Delta T \approx 3$  K, no primary phase is seen (Fig. 1), and when  $\Delta T \approx 51$  K (Fig. 6), both epitaxial growth of the NiSi phase on the NiSi<sub>2</sub> phase and epitaxial growth of the NiSi<sub>2</sub> phase on the NiSi phase are seen, a specific EOR is also available. The present work and the previous work on EORs [10–24] show that eutectic growth obeys the specific EORs and the EORs significantly influence the eutectic morphologies. It should be noted that no globally representative EOR is identified for either the unmodified or Sr-modified Al–12.7wt.%Si alloys in the work of LIU et al [19], according to which crystallographic compatibility across the phase interface is not a prerequisite for the formation of Al–Si eutectics. A detailed study of Fig. 6(b) in Ref. [19], however, indicates that there are multiple EORs between  $\alpha(\text{Al})$  and Si, similar to the case when  $\Delta T \approx 31$  K in the current study.

#### 4.2 Multiple EORs vs single EOR

As stated in the introduction section, there are usually multiple EORs between two eutectic phases rather than just one, and under the effects of a high magnetic field, the EOR can change from one to another. In the present work, seven EORs are found between the NiSi and NiSi<sub>2</sub> phases and one case presents multiple EORs. For the lamellar eutectics seen when  $\Delta T \approx 3, 15, 31$  and 51 K, coupled eutectic growth prevails, whereas for the eutectic dendrites seen when  $\Delta T \approx 74$  K, uncoupled eutectic growth occurs [9]. Therefore, the possible change in the growth direction of the primary phase in undercooled melts [33,34], the change of primary phase from the NiSi phase to the NiSi<sub>2</sub> phase, and the transition from coupled eutectic growth to uncoupled eutectic growth can be the reasons for the current multiple EORs. For example, after nucleation or epitaxial growth of one eutectic phase, the epitaxial growth of the second eutectic phase depends not only on the phase but also on the

orientation of the primary eutectics, thus significantly influencing the dominated EOR.

A single EOR or multiple EORs can be dominant, possibly depending on the crystallographic character of the primary eutectic phase. In the present work, a single EOR is found when  $\Delta T \approx 3, 15$  and 74 K, and three EORs are found when  $\Delta T \approx 31$  K. To the best of authors' knowledge, multiple EORs in one sample were reported for directional solidification or casting of unmodified and modified Al–Si alloys [16–19], where twin-controlled growth of the eutectic Si phase occurred on the primary Al phase. Since the twinning relationship is found within either a dendritic [18] or lath-shaped [19] Si grain, whereas grains A, B and C in Fig. 3 of the present work belong to different grains, the present triple EORs seem to be unique. In the case of a Mg-modified Nb–Si alloy [20], there are total eleven EORs in one sample; since the eutectic reaction is followed by a eutectoid reaction, it is not possible to retain the primary solidification microstructure that shows the original EORs during solidification. In contrast, the current work shows, without any controversy, that epitaxial growth of the second eutectic phase on the primary eutectic phase can obey either a single EOR or multiple EORs and thus helps understand eutectic growth and eutectic morphologies.

#### 5 Conclusions

(1) There are multiple EORs in the undercooled Ni–38wt.%Si eutectic alloy and seven EORs are characterized in five different microstructures. Three EORs co-exist when  $\Delta T \approx 31$  K, in which the orientation of the primary NiSi phase is the same but the misorientation between the neighboring NiSi<sub>2</sub> grains can be either 50° or 60°. There is however no clear relationship between undercooling and the EOR(s).

(2) The EORs for the epitaxial growth of the NiSi phase on the NiSi<sub>2</sub> phase and the epitaxial growth of the NiSi<sub>2</sub> phase on the NiSi phase can be the same if the magnitude of undercooling is the same. The EORs of epitaxial growth of the NiSi phase on the NiSi<sub>2</sub> phase can be different and diverse if the magnitude of undercooling (or microstructure) is different, even for cases where the solidification conditions are similar.

(3) A possible change in the growth direction of the primary phase in undercooled melts, the change of the primary phase from the NiSi phase to the NiSi<sub>2</sub> phase, and the transition from coupled to uncoupled eutectic growth are the reasons for the current multiple EORs. The current work shows, without any controversy, that epitaxial growth of the second eutectic phase on the primary eutectic phase can obey either a single EOR or multiple EORs. Such a phenomenon is unique in our understanding of cooperative growth, further theoretical analysis of which will improve current eutectic growth theory and might play an important role in microstructural control.

(4) Though both the present work and previous work on EORs show that eutectic growth obeying specific EOR(s) and the EOR(s) can significantly influence the eutectic morphologies, the EOR is only one of the eight factors that may influence the eutectic morphologies. It helps understand the eutectic microstructures but cannot be assumed to be the only effect that dominates eutectic morphologies.

## References

- [1] HERLACH D M. Non-equilibrium solidification of undercooled metallic melts [J]. *Materials Science and Engineering R*, 1994, 12: 177–272.
- [2] LI J F, ZHOU Y H. Eutectic growth in bulk undercooled melts [J]. *Acta Materialia*, 2005, 53: 2351–2359.
- [3] WANG H F, LIU F, HERLACH D M. Kinetics of triple-junctions in eutectic solidification: A sharp interface model [J]. *Journal of Materials Science*, 2015, 50: 176–188.
- [4] KUANG W W, WANG H F, LIU F, SOBOLEV S L. Modeling of eutectic dendrite growth in undercooled binary alloys [J]. *Journal of Materials Science*, 2016, 51: 2141–2152.
- [5] WEI B, HERLACH D M, SOMMER F. Rapid eutectic growth of undercooled metallic alloys [J]. *Journal of Materials Science Letters*, 1993, 12: 1774–1777.
- [6] CLOPET C R, COCHRANE R F, MULLIS A M. The origin of anomalous eutectic structures in undercooled Ag–Cu alloy [J]. *Acta Materialia*, 2013, 61: 6894–6902.
- [7] LI Xin-zhong, LIU Dong-mei, SUN Tao, SU Yan-qing, GUO Jing-jie, FU Heng-zhi. Phase-field simulation of lamellar growth for a binary eutectic alloy [J]. *Transaction of Nonferrous Metals Society of China*, 2010, 20: 302–307.
- [8] QUE Z P, GU J H, SHIN J H, LEE J H. Microstructure transition from stable to metastable eutectic growth in Ni–25%Al alloy [J]. *Transaction of Nonferrous Metals Society of China*, 2014, 24: 106–111.
- [9] LAI C, WANG H F, PU Q, XU T T, YANG J S, ZHANG X, LIU F. Phase selection and re-melting-induced anomalous eutectics in undercooled Ni–38wt%Si alloys [J]. *Journal of Materials Science*, 2016, 51: 10990–11001.
- [10] RAMIREZ-RICO J, LOPEZ A R A, FERNANDEZ J M, PENA J I, LARREA A. Crystallographic texture in Al<sub>2</sub>O<sub>3</sub>–ZrO<sub>2</sub> (Y<sub>2</sub>O<sub>3</sub>) directionally solidified eutectics [J]. *Journal of the European Ceramic Society*, 2008, 28: 2681–2686.
- [11] ZABALETA S S, BERCERO M A L, MARTIN L O S, LARREA A. Orientation relationships and interfaces in directionally solidified eutectics for solid oxide fuel cell anodes [J]. *Journal of the European Ceramic Society*, 2014, 34: 2123–2132.
- [12] WITUSIEWICZ V T, HECHT U, REX S. In-situ observation of eutectic growth in Al-based alloys by light microscopy [J]. *Journal of Crystal Growth*, 2013, 372: 57–64.
- [13] BONNET R, DURAND F. Geometric discussion of the relationships between the phases Al and Al<sub>2</sub>Cu for the eutectic and precipitates of CuAl<sub>2</sub> [C]/Proceedings of the Conference on In-situ Composites. Lakerville, USA: National Academy of Science, 1973: 209–223.
- [14] FAN Y Y, MAKHLOUF M M. The Al–Al<sub>3</sub>Ni eutectic reaction: Crystallography and mechanism of formation [J]. *Metallurgical and Materials Transactions A*, 2015, 46: 3808–3812.
- [15] HERTZBERG R W, LEMKEY F D, FORD J A. Mechanical behavior of lamellar (Al–CuAl<sub>2</sub>) and whisker type (Al–Al<sub>3</sub>Ni) unidirectionally-solidified eutectic alloys [J]. *Transactions of the Metallurgical Society of AIME*, 1965, 233: 342.
- [16] MAZAHERY A, SHABANI M O. Modification mechanism and microstructural characteristics of eutectic Si in casting Al–Si alloys: A review on experimental and numerical studies [J]. *JOM*, 2014, 66: 726–738.
- [17] HEIBERG G, ARNBERG L. Investigation of the microstructure of the Al–Si eutectic in binary aluminium–7 wt% silicon alloys by electron backscatter diffraction (EBSD) [J]. *Journal of Light Metals*, 2001(1): 43–49.
- [18] PATAKHAM U, KAJOMCHAAIYAKUL J, LIMMANE-UVICHITR C. Modification mechanism of eutectic silicon in Al–6Si–0.3Mg alloy with scandium [J]. *Journal of Alloys and Compounds*, 2013, 575: 273–284.
- [19] LIU X R, ZHANG Y D, BEAUSIR B, LIU F, ESLING C, YU F X, ZHAO X, ZUO L. Twin-controlled growth of eutectic Si in unmodified and Sr-modified Al–12.7%Si alloys investigated by SEM/EBSD [J]. *Acta Materialia*, 2015, 97: 338–347.
- [20] MIURA S, OHKUBO K, MOHRI T. Microstructural control of Nb–Si alloy for large Nb grain formation through eutectic and eutectoid reactions [J]. *Intermetallics*, 2007, 15: 783–790.
- [21] LI X, FAUTRELLE Y, REN Z M, ZHANG Y D, ESLING C. Effect of a high magnetic field on the Al–Al<sub>3</sub>Ni fiber eutectic during directional solidification [J]. *Acta Materialia*, 2010, 58: 2430–2441.
- [22] LI X, REN Z M, FAUTRELLE Y, ZHANG Y D, ESLING C. Morphological instabilities and alignment of lamellar eutectics during directional solidification under a strong magnetic field [J]. *Acta Materialia*, 2010, 58: 1403–1417.
- [23] LI X, REN Z M, FAUTRELLE Y, ZHANG Y D, ESLING C.

- Effects on high magnetic fields on the microstructure of Al–Al<sub>2</sub>Cu eutectic [J]. *Materials Letters*, 2010, 64: 2597–2600.
- [24] GENAU A L, RATKE L. Crystal orientation and morphology in Al–Ag–Cu ternary eutectic [J]. *Materials Science and Engineering*, 2011, 27: 012032.
- [25] NASH P, NASH A. The Ni–Si (nickel–silicon) system [J]. *Journal of Phase Equilibria*, 1987, 8: 6–14.
- [26] WEI X X, LIN X, XU W. Remelting-induced anomalous eutectic formation during solidification of deeply undercooled eutectic alloy melts [J]. *Acta Materialia*, 2015, 95: 44–56.
- [27] SCHWARZ M, KARMA A, ECKLER K, HERLACH D M. Physical mechanism of grain refinement in solidification of undercooled melts [J]. *Physical Review Letters*, 1994, 73: 1380–1383.
- [28] GOETZINGER R, BARTH M, HERLACH D M. Mechanism of formation of the anomalous eutectic structure in rapidly solidified Ni–Si, Co–Sb and Ni–Al–Ti alloys [J]. *Acta Materialia*, 1998, 46: 1647–1655.
- [29] AHMAD R, COCHRANE R F, MULLIS A M. The formation of regular  $\alpha$ Ni– $\gamma$ (Ni<sub>31</sub>Si<sub>12</sub>) eutectic structures from undercooled Ni–25at.%Si melts [J]. *Intermetallics*, 2012, 22: 55–61.
- [30] CAO L G, COCHRANE R F, MULLIS A M. Lamella structure formation in drop-tube processed Ni–25.3at.%Si alloy [J]. *Journal of Alloys and Compounds*, 2014, 615(S): s599–s601.
- [31] GOGEBAKAN M, KURSUN C, GUNDUZ K O, TARAKCI M, GENCER Y. Microstructural and mechanical properties of binary Ni–Si eutectic alloys [J]. *Journal of Alloys and Compounds*, 2015, 643(S): s219–s225.
- [32] WANG H F, LIU F, YANG G C. Experimental study of grain refinement mechanism in undercooled Ni–15at.%Cu alloy [J]. *Journal of Materials Research*, 2010, 25: 1963–1974.
- [33] CASTLE E G, MULLIS A M, COCHRANE R F. Evidence for an extensive, undercooling-mediated transition in growth orientation, and novel dendritic seaweed microstructures in Cu–8.9 wt.% Ni [J]. *Acta Materialia*, 2014, 66: 378–387.
- [34] CASTLE E G, MULLIS A M, COCHRANE R F. Mechanism selection for spontaneous grain refinement in undercooled metallic melts [J]. *Acta Materialia*, 2014, 77: 76–84.
- [35] BRAGARD J, KARMA A, LEE Y H, PLAPP M. Linking phase-field and atomistic simulations to model dendritic solidification in highly undercooled melts [J]. *Interface Science*, 2002, 10: 121–136.
- [36] AKAMATSU S, NGUYEN T H. In situ observation of solidification patterns in diffusive conditions [J]. *Acta Materialia*, 2016, 108: 325–346.
- [37] ZHAO B, VERHASSELT J C, SHVINDLERMAN L S, GOTTSTEIN G. Measurement of grain boundary triple line energy in copper [J]. *Acta Materialia*, 2010, 58: 5646–5653.
- [38] ZHAO B, ZIEMONS A, SHVINDLERMAN L S, GOTTSTEIN G. Surface topography and energy of grain boundary triple junctions in copper tricrystals [J]. *Acta Materialia*, 2012, 60: 811–818.
- [39] AKAMATSU S, PLAPP M, FAIVRE G, KARMA A. Pattern stability and trijunction motion in eutectic solidification [J]. *Physical Review (E): Statistical, Nonlinear, and Soft Matter Physics*, 2002, 66: 030501.
- [40] AKAMATSU S, PLAPP M, FAIVRE G, KARMA A. Overstability of lamellar eutectic growth below the minimum-undercooling spacing [J]. *Metallurgical and Materials Transactions A*, 2004, 35: 1815–1828.
- [41] LANGER J S. Eutectic solidification and marginal stability [J]. *Physical Review Letters*, 1980, 44: 1023–1026.
- [42] DATYE V, LANGER J S. Stability of thin lamellar eutectic growth [J]. *Physical Review B*, 1981, 24: 4155–4169.

## 过冷 Ni–38%Si 共晶合金中的多重共晶取向关系

张帆<sup>1</sup>, 王海丰<sup>1</sup>, 赖存<sup>2</sup>, 张建宝<sup>1</sup>, 张雅婵<sup>1</sup>, 周青<sup>1</sup>

1. 西北工业大学 凝固技术国家重点实验室 先进润滑与密封材料研究中心, 西安 710072;

2. 中国航天科工集团公司第三研究院, 北京 100074

**摘要:** 采用电子背散射衍射技术分析过冷 Ni–38%Si(质量分数)合金中的共晶取向关系, 发现在过冷 Ni–38%Si(质量分数)合金中总共存在 7 种共晶取向关系。当过冷度 $\Delta T \approx 31$  K 时, 存在 3 种共晶取向关系, 其初生 NiSi 相的取向相同, 但相邻 NiSi<sub>2</sub> 晶粒之间的取向差约为 50°或 60°。多重共晶取向关系的产生归因于初生相生长方向的变化、初生相从 NiSi 相到 NiSi<sub>2</sub> 相的变化以及生长方式从耦合共晶生长到非耦合共晶生长的转变。第二共晶相外延生长于初生共晶相时可以遵循一种共晶取向关系或多种共晶取向关系, 这是一种较为独特的现象。

**关键词:** 共晶取向关系; 外延生长; 过冷; Ni–Si 合金

(Edited by Wei-ping CHEN)